**PASJ:** Publ. Astron. Soc. Japan **59**, S807–S813, 2007 November 30


# Flare Ribbons Observed with G-band and Fe I 6302 Å Filters of the Solar Optical Telescope on Board Hinode*

Hiroaki ISOBE,[1] Masahito KUBO,[2,3] Takashi MINOSHIMA,[1] Kiyoshi ICHIMOTO,[4] Yukio KATSUKAWA,[4] Theodore D. TARBELL,[5] Saku TSUNETA,[4] Thomas E. BERGER,[5] Bruce LITES,[2] Shin'ichi NAGATA,[6] Toshifumi SHIMIZU,[3] Richard A. SHINE,[5] Yoshinori SUEMATSU,[4] and Alan M. TITLE[5]

[1]*Department of Earth and Planetary Science, The University of Tokyo, 7-3-1 Hongo, Bunkyo-ku, Tokyo 113-0033*
*isobe@eps.s.u-tokyo.ac.jp*

[2]*High Altitude Observatory, National Center for Atmospheric Research, P O Box 3000, Boulder, CO 80307, USA*

[3]*Institute of Space and Astronautical Science, Japan Aerospace Exploration Agency, 3-1-1 Yoshinodai, Sagamihara, Kanagawa 229-8510*

[4]*National Astronomical Observatory of Japan, 2-21-1 Osawa, Mitaka, Tokyo 181-8588*

[5]*Lockheed Martin Solar and Astrophysics Center, Bldg. 252, 3251 Hanover Street, Palo Alto, CA 94304, USA*

[6]*Hida Observatory, Kyoto University, Takayama, Gifu 506-1314*

(Received 2007 August 16; accepted 2007 September 11)

**Abstract**

The Solar Optical Telescope (SOT) on board the Hinode satellite observed an X3.4 class flare on 2006 December 13. A typical two-ribbon structure was observed, not only in the chromospheric Ca II H line, but also in the G-band and Fe I 6302 Å line. The high-resolution, seeing-free images achieved by SOT revealed, for the first time, sub-arcsec fine structures of the "white light" flare. The G-band flare ribbons on sunspot umbrae showed a sharp leading edge, followed by a diffuse inside, as well as a previously known core–halo structure. The underlying structures, such as umbral dots, penumbral filaments, and granules, were visible in the flare ribbons. Assuming that the sharp leading edge was directly heated by a particle beam and the diffuse parts were heated by radiative back-warming, we estimated the depth of the diffuse flare emission using an intensity profile of the flare ribbon. We found that the depth of the diffuse emission was about 100 km or less from the height of the source of radiative back-warming. The flare ribbons were also visible in the Stokes-$V$ images of Fe I 6302 Å, as a transient polarity reversal. This is probably related to a "magnetic transient" reported in the literature. The intensity increase in Stokes-$I$ images indicates that the Fe I 6302 Å line was significantly deformed by the flare, which may cause such a magnetic transient.

**Key words:** Sun: chromosphere — Sun: flares — Sun: photosphere

## 1. Introduction

Solar flares that are visible in the optical continuum are called white light flares (WLFs). They have been of interest because the radiative loss by the WL emission is significant, they are similar to stellar flares in many aspects, and their energy transport and emission mechanisms have been challenging problems (Neidig 1989). Observers used to believe that WL emissions are seen only in the most energetic flares (Hiei 1982; Neidig 1989). However, seeing-free observations from spacecrafts have revealed that even C-class flares show an enhancement in the optical continuum (Matthews et al. 2003; Hudson et al. 2006).

Close correlations in space and time between WL and hard X-ray (HXR) emissions have been reported in many events, strongly suggesting that WLFs are energized by nonthermal electron beams (Rust & Hegwer 1975; Hudson et al. 1992; Neidig & Kane 1993; Chen & Ding 2006). Recently, several authors studied the energetics of WLFs, while examining whether a nonthermal electron beam had sufficient energy to power the WLFs (Metcalf et al. 2003; Chen & Ding 2006; Fletcher et al. 2007). Their results indicate that, for most WLFs, the energy required to power the WL emission was comparable to the total energy carried by the electron beam, and therefore the WLFs were energized by low-energy electrons, about 20 keV or less, which carried most of the energy. Such low-energy electrons cannot penetrate into the photosphere or lower chromosphere, so they deposit energy in the upper chromosphere (Hudson et al. 1972). Hence, the WL emission may also come from the upper chromosphere, or the energy is transported by radiation into a deeper layer where the WL emission occurs (so-called back-warming effect; Machado et al. 1989; Metcalf et al. 1990).

The morphology also gives some clues to examine the mechanisms of WLFs. High-resolution images often show the separation of a WLF kernel into a bright inner core and a fainter outer region (halo) (Neidig et al. 1993; Hudson et al. 2006). Using high-cadence ground based observations, Xu et al. (2006) examined the timing of WL and HXR emissions in the core and halo separately. They found that the peak of WL in the halo showed a delay from that of HXR, but they

* Movies for figures 2 and 4 are available in the electronic version ⟨http://pasj.asj.or.jp/v59/sp3/59s335/⟩.

were almost simultaneous in the core. This suggests direct heating by electron beams in the core and indirect heating by back-warming (or something else) in the halo.

The high-resolution, seeing-free images from the Solar Optical Telescope (SOT: Tsuneta et al. 2007) aboard Hinode (Kosugi et al. 2007) provide a qualitatively new data set for studying WLFs. After its launch in 2006 September, Hinode has successfully observed several flares. The X3.4 flare on 2006 December 13 was of particular interest from the view point of WLF, because the SOT observed two clear ribbons, not only in the chromospheric Ca II H images, but also in the G-band images and the Stokes $I$ and $V$ images of the Fe I 6302 Å line. The G-band and the Fe I 6302 lines are not "white light" in a strict sense, but they both originate in the photosphere. Moreover, the flare emission seen in Stokes $V$ images may be related to so-called magnetic transients (magnetic anomalies), the transient signals in magnetograms associated with WLFs, whose origin remains uncertain (Patterson & Zirin 1981; Zirin & Tanaka 1981; Kosovichev & Zharkova 2001; Qiu & Gary 2003). The aim of this paper is to present the initial SOT observation of the flare ribbons of this event and to discuss their possible indications for the mechanisms of WLFs.

## 2. Observation

### 2.1. Data

The X3.4-class flare on 2006 December 13 in active region NOAA 10930 was observed by all three instruments aboard Hinode: the SOT, the Extreme-ultraviolet Imaging Spectrometer (EIS: Culhane et al. 2007), and the X-Ray Telescope (XRT: Golub et al. 2007). Kubo et al. (2007) studied the long-term evolution of the vector magnetic field of this region using the SOT data.

The aperture of SOT is 50 cm and is the largest for an optical telescope ever built to observe the Sun from space. An initial investigation showed that SOT achieved its diffraction limit, 0.″2–0.″3. SOT performs both filter and spectral observations at high polarimetric precision (Ichimoto et al. 2007). The Spectro-Polarimeter (SP) obtains full Stokes profiles of the magnetic sensitive Fe I 6302 Å line. The Filtergram (FG) observation has two channels, namely the Broadband Filter Imager (BFI) and the Narrowband Filter Imager (NFI). BFI has 6 broad bands (CN band, Ca II H line, G-band, and 3 continuum bands) and obtains photometric images with 0.″0542 pixel$^{-1}$ sampling. NFI provides intensity, Doppler, and Stokes polarimetric imaging with 0.″08 pixel$^{-1}$ sampling. There are 10 available spectral lines, including Fe lines with different magnetic sensitivity, Mg I b, Na I D, and H$\alpha$. For instrumental details of SOT, see Tsuneta et al. (2007), Suematsu et al. (2007), Ichimoto et al. (2007), and Shimizu et al. (2007).

The SOT/FG observation has a large degree of freedom: choice of filters, field of view (FOV), pixel summing, cadence, etc. During the flare, BFI obtained Ca II H and G band images with a full field of view of 218″ × 109″, 2 × 2 summing, and 2 min cadence. No continuum band images were taken during this flare. NFI obtained the intensity (Stokes-$I$) and circular polarization (Stokes-$V$) at −120 mÅ from the line center of the photospheric line Fe I 6302. Hereafter, we refer to them as 6302 $I$ and 6302 $V$ images, respectively. The FOV, pixel summing, and cadence of NFI were 328″×164″, 2 × 2, and 2 min, respectively. Eight exposures during polarization modulation were used to obtain a set of 6302 $I$ and 6302 $V$ images, which took about 14 s. This resulted in some blurring of the image, particularly when sharp structures were moving rapidly, as is the case of flare ribbons.

The 6302 $V$ images provide a proxy for line-of-sight magnetograms. The line-of-sight magnetic field $B_{\rm l}$ is approximately given by

$$B_{\rm l} = -\frac{C_V}{0.798 C_I} \times 10000\ ({\rm G}), \tag{1}$$

where $C_I$ and $C_V$ are the counts of the 6302 $I$ and 6302 $V$ images, respectively, and $C_V/0.798$ gives the circular polarization (Stokes-$V$). This approximation is crude and breaks down for large $B_{\rm l}$. For example, $C_V$ in the umbrae is smaller than that in the penumbrae.

Figure 1 shows a Ca II H image and a running difference of G-band images. The flare occurred between two umbrae that have opposite polarities, where strong shearing motion was found (Kubo et al. 2007). The Ca II H image shows two large ribbons that extend nearly 200″ along the polarity inversion line. Unfortunately, the exposure was not optimized for a flare, and hence the brightest parts of the Ca II H ribbons were saturated. The G-band images also show clear ribbon structures, but they were visible only for some parts of the Ca II H ribbon. Indeed the G-band ribbons were co-spatial with the saturated, i.e., the brightest, parts of the Ca II H ribbon, as indicated by box A (upper sunspot), box B (lower sunspot), and box C (outside sunspots) in figure 1. The flare ribbons were also visible in 6302 $I$ and 6302 $V$ with less spatial extent. In the following we examine the fine structures in the different parts of the ribbons.

### 2.2. Ribbon in the Northern Sunspot

Figure 2 shows G band, 6302 $I$, and 6302 $V$ images of the ribbon in the northern sunspot. The times of the images were 02:24, 02:28 and 02:32, and the FOV was the same as box A in figure 1 (see also movie 1). The remarkable feature is a sharp leading edge, followed by a diffuse inside. The leading edge and the diffuse inside look similar to the core–halo structure found in previous observations (Neidig et al. 1993; Hudson et al. 2006), but such a sharp and coherent leading edge has not been seen before. The leading edge is sharpest in the G band, and also visible in 6302 $I$, but not clear in 6302 $V$.

The intensity profiles along the vertical dotted line in figure 2 are shown in figure 3. The diamonds are those at 02:28, and the plus signs are those at 02:20. The peak intensity on the leading edge is 600% larger than the pre-flare intensity in the G band, and 50% larger in 6302 $I$. The 6302 $V$ count reverses the sign, from ∼100 in the pre-flare umbra to ∼−170 at the peak. The sign reversal is transient and occurred only when and where the flare ribbon was also visible in 6302 $I$. Therefore, it is very unlikely to be a real magnetic field change.

The flare ribbon was also visible in the penumbra, as indicated by the arrows in figure 2. By comparison of the images at different time, one can recognize the same

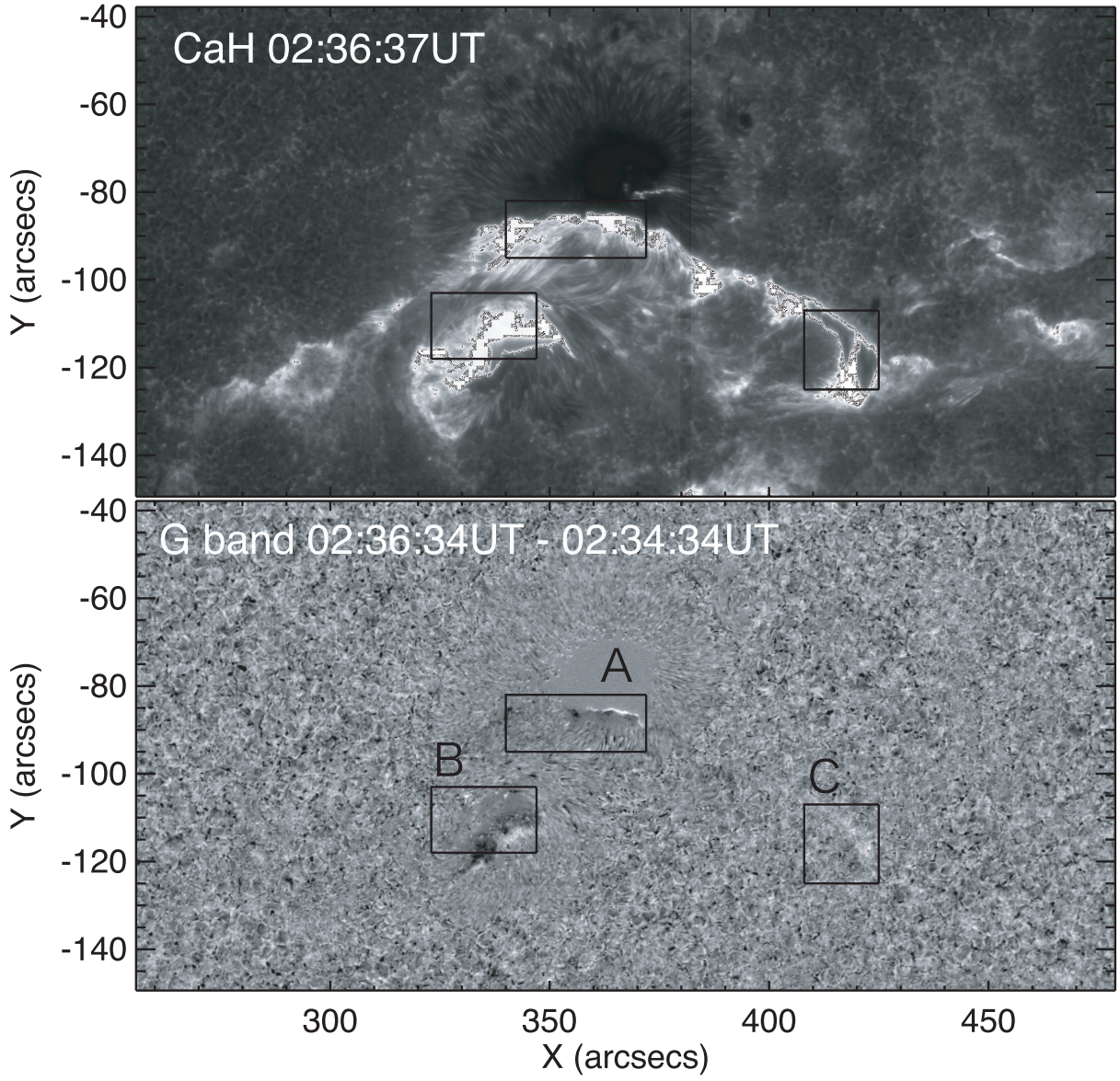


**Fig. 1.** Upper panel: Ca II H image of the X3.4 flare on 2006 December 13. Lower panel: running difference of the G-band images.

filamentary structure of the penumbra in the flare ribbon, both in the G-band and in 6302 $I$. This gives us an impression that the flare components seen in these filters were optically thin. The intensity increase in penumbral flare ribbon was $\sim 50\%$ for the G-band and $\sim 10\%$ for 6302 $I$. The 6302 $V$ images also show the flare ribbon in the penumbra. It did not change the sign, but decreased significantly in magnitude, typically from 500 to 300.

### *2.3. Ribbon in the Southern Sunspot*

Figure 4 shows G-band images of the flare ribbon on the southern sunspot (also see movie 2)*. The FOV is the same as box B in figure 1. The leading-edge and diffuse-inside structure is also seen, but there are more patchy bright points compared with the ribbon in the northern sunspot. Note that in this sunspot there are many umbral dots, which are almost absent in the northern sunspot. Many of the bright points in the flare ribbon seen at 02:28 UT are co-spatial with the umbral dot seen before (02:24) and after (02:32) the ribbon passage. One example is indicated as "UD" in figure 4. Hence, these bright points are not the intrinsic structure of the flare emission.

However, some bright points are not the underlying umbral dots. An example is indicated as "FK" in figure 4. The intensity profiles across the umbral dot "UD" and the flare kernel "FK" (along the white lines with a gap in the middle) are shown in panel (d) of figure 4. Contrary to UD, FK shows no enhancement before and after the ribbon passage. Therefore, these flare kernels are not due to the pre-flare atmospheric structure, but indeed due to the fine structure in the flare energy deposition. The FWHM of the FK is about 300 km, but we cannot rule out the existence of unresolved finer structure.

The 6302 $I$ images (not shown) were similar to those in

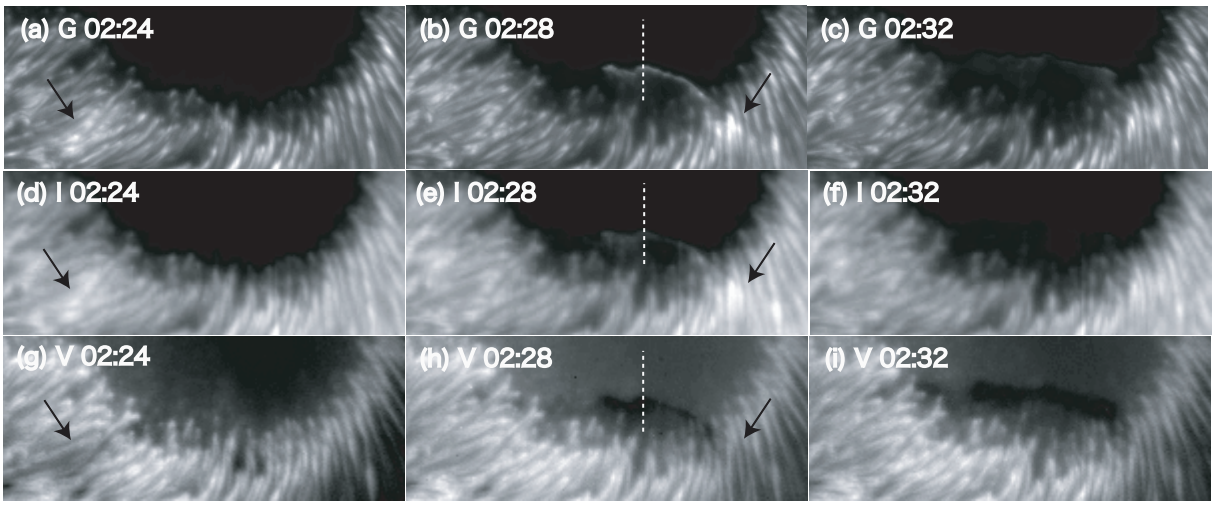


**Fig. 2.** Snapshots of flare ribbons in the northern sunspots in the G band (panels a–c), 6302 $I$ (panels d–f), and 6302 $V$ (panels g–i). The FOV is the same as box A in figure 1, and the times of the images are indicated in the figure. The arrows indicate the flare ribbon in the penumbra. The intensity profiles along the dashed vertical lines are plotted in figure 3. A movie is provided as an on-line material (movie 1).*

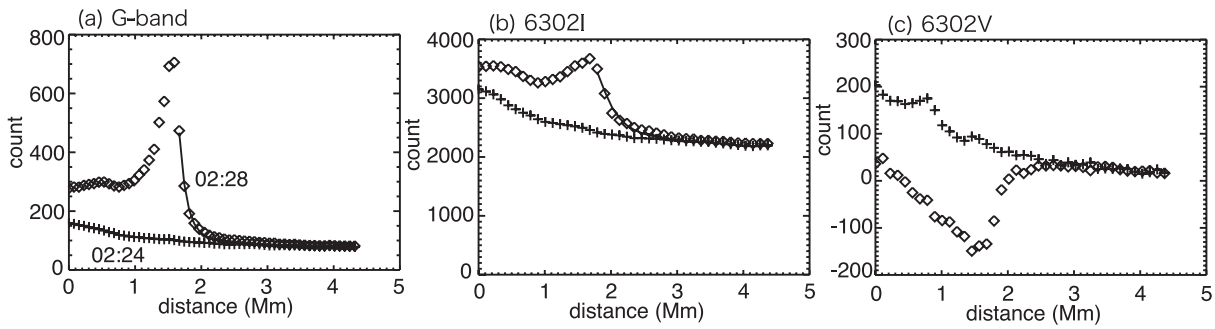


**Fig. 3.** Intensity profiles along the vertical line in figure 2. Plus signs and diamonds correspond to 02:24 UT (preflare) and 02:28 UT (during flare), respectively. The solid lines shows the best-fit model; see subsection 3.1.

the G band, showing umbral dots, flare kernels, and diffuse ribbon, although the spatial resolution was less, and the images appeared more blurred. In 6302 $V$ images, the diffuse ribbon was seen, but the flare kernels were unclear. It also showed sign reversal, where the flare ribbon was bright in 6302 $I$.

### 2.4. *Ribbon outside the Sunspot*

The flare ribbon was also visible outside the sunspot, as shown in figure 5. The FOV is the same as box C in figure 1. Panels (a) and (b) show successive G-band images in which the flare ribbon can be seen. The intensity increase in the flare ribbon is 10–20%, which is comparable to the contrast of the background granulation. The flare ribbon is more clearly seen in the differenced image (panel c). It should be noted that the underlying granules are visible in the flare ribbon. The flare ribbon looks diffuse, but the existence of fine structures is difficult to address because of the underlying granules.

Panel (d) of figure 5 shows a difference image of 6302 $I$ at almost the same time as the G-band difference image. The intensity increase is about 5%. We could not recognize the flare ribbon in 6302 $V$ images in this region.

## 3. Discussion

### 3.1. *Height of the Flare Emission*

The height of the WLF emission is closely related to the transport and emission mechanisms. The striking sharpness of the fine structures in the flare ribbons found by SOT allows us to put a constraint on their vertical structure, as discussed below. It seems reasonable to believe that the sharp leading edge and diffuse inside found in the present event may be an analog of the core–halo structure found in previous observations (Neidig et al. 1993; Hudson et al. 2006; Xu et al. 2006). Assuming that the interpretation of Xu et al. (2006) can be applied to our event, i.e., direct heating by particle beams in the core (leading edge) and radiative back-warming in the halo (diffuse part), we made a simple model to measure the upper limit of the depth of the layer at which the diffuse emission occurs. The intensity profiles plotted in figure 3 show that there is a tail outside the leading edge. We assume that the flare energy is deposited only at the peak of the leading edge, and subsequent back-warming by the irradiation from the peak produces the outside tail. Using the intensity profile of the

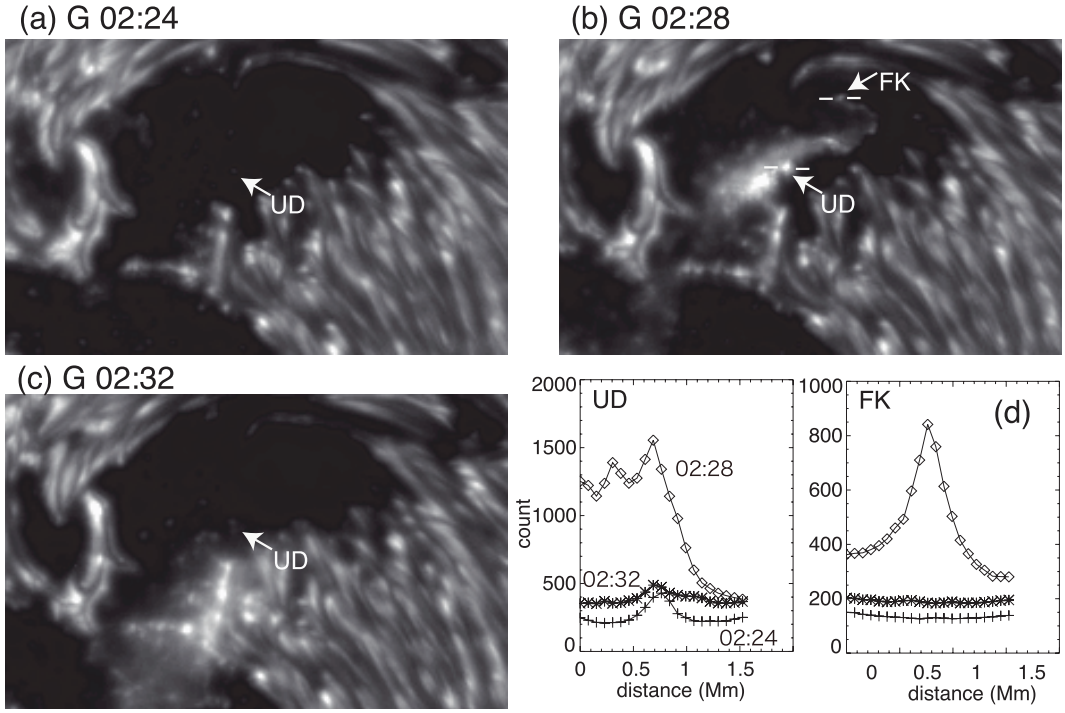


**Fig. 4.** (a)–(c) G-band images of the flare ribbon in the southern sunspot. FOV is the same as box B in figure 1. (d) Intensity profiles of the umbral dot (marked as UD) and the flare kernel (marked as FK). A movie is prvided as an on-line material (movie 2).*

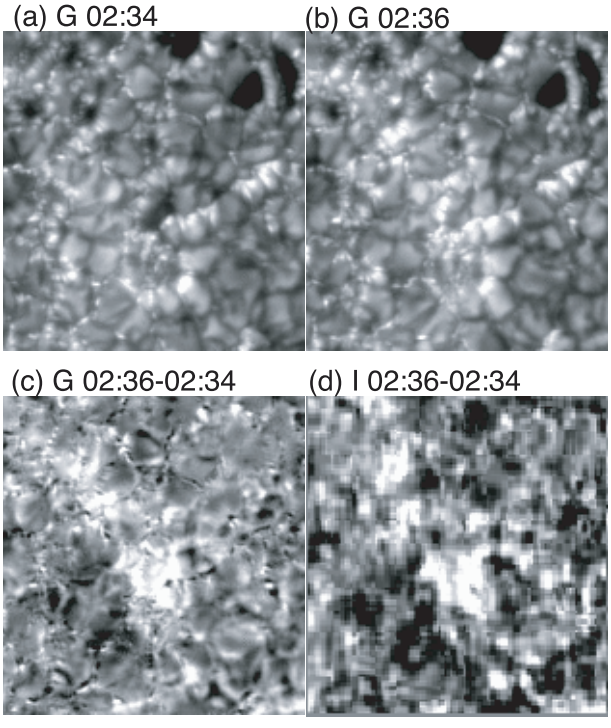


**Fig. 5.** (a)–(b) G-band images of the flare ribbon outside the sunspots. FOV is the same as box C in figure 1. (c) Difference image of G band. (c) Difference image of 6302 $I$.

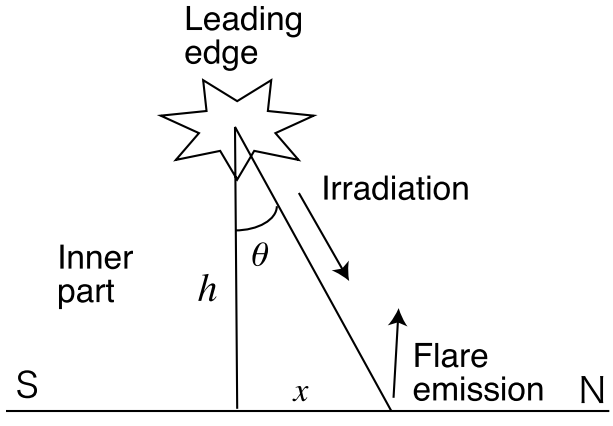


**Fig. 6.** Schematic illustration of the model.

outside tail, we can derive the depth of the diffuse emission layer relative to the irradiating source. To do this, we make several more assumptions: (1) Any variation along the flare ribbon is neglected, i.e., the system is two-dimensional, (2) The pre-flare atmosphere is uniform, (3) The irradiation is isotropical. (4) The source of irradiation is a one-dimensional line whose thickness is negligibly small. Thus, we neglect irradiation from the inner part of the ribbon. (5) The diffuse emission from the outside tail comes from an infinitely thin layer with fixed geometrical height, at which the irradiating photons are absorbed. (6) Absorption of the irradiating photons between this layer and the irradiating source is negligible.

The model is illustrated in figure 6. Here, $h$ denotes the depth of the flaring layer by back-warming, measured from the irradiation source; $x$ is the distance from the irradiation source projected on the flaring layer, and $\theta$ is the angle from the vertical. Then the intensity outside the leading edge $I(x)$ is

given by

$$I(x) = \alpha J \frac{d\theta}{dx} + I_0 = \frac{\alpha J h}{x^2 + h^2} + I_0 \quad (x > 0) \tag{2}$$

and

$$I(x = 0) = \frac{\alpha J}{h} + I_0 + I_{\rm p}, \tag{3}$$

where $J$ is the energy of irradiation per unit length and per radian, $I_0$ is the preflare intensity, and $\alpha$ is a coefficient. $I_{\rm p}$ is an extra component at the leading edge that comes from the initial energy deposition layer. We determined the parameters $\alpha J/h$ and $h$ by a least-squares fitting of the intensity profile of the ribbon at 02:28, shown in figure 2. Note that $I_{\rm p}$ is not a free parameter, because it can be calculated from the observed peak intensity once $\alpha J/h$ and $h$ are determined.

The solid lines in panels (a) and (b) of figure 3 are the results of fittings. The best-fit parameters are $h = 124$ km and $\alpha J/h = 528$ counts for the G band, and $h = 300$ km and $\alpha J/h = 1385$ counts for 6302 $I$. These values of $h$ are actually upper limits. First of all, $h = 124$ km for the G band is comparable to the diffraction limit of the telescope. In addition, there may be an effect of long-range scattered light that has not be investigated. Such effects unsharpen the images, and therefore cause an overestimate of $h$. For 6302 $I$, $h = 300$ km is well above the diffraction limit. But, as already mentioned, 6302 $I$ images suffer significant blurring due to rapid motion of the flare ribbon. The apparent velocity of the flare ribbon is roughly about 7 km s$^{-1}$. During 14 s (time to obtain a 6302 $I$ image) the flare ribbon moves by about 100 km, which possibly caused the larger $h$ for 6302 $I$. Furthermore, the effects of projection (not significant because the flare occurs close to the equator) and irradiation from the inner part of the ribbon (may be significant) were not taken into account, which also resulted in an overestimate of $h$. Thus, the sharpness of the leading edge of the flare ribbon indicates that the depth of the diffuse ribbon measured from the irradiation source ($\sim$ energy deposition height) is on the order of 100 km, or even less.

Such a small value of $h$ (i.e., smaller the local scale height $\approx 200$ km) indicates that assumptions (5) and (6) are probably irrelevant approximations, because the opacity for the irradiating photons is unlikely to significantly change at such a small depth. In order to examine the effect of absorption, we tried to fit the intensity profile with an absorption factor, namely

$$I(x) = \frac{\alpha J h}{x^2 + h^2} \exp\left(-b\sqrt{x^2 + h^2}\right) + I_0 \quad (x > 0), \tag{4}$$

where $b$ is related to the absorption coefficient. The absorption factor reduces the intensity far away from the irradiating source, and hence fitting with this factor would result in a larger $h$. However, the least-squares fitting yielded $b = 0$, i.e., no absorption. As a consequent, the best-fit values of $h$ and $J/h$ are the same. More accurate modeling requires a proper treatment of the radiative transfer and emission mechanisms, but we believe that our simple model gives roughly the correct depth of the WL emission.

The actual height of the flare emission in the solar atmosphere is uncertain because we do not know the height of the irradiation source. However, previous studies suggest that the WLF emission is powered by relatively low ($\lesssim 20$ keV) electrons, and hence the energy deposition layer is in the upper chromosphere (Metcalf et al. 2003; Chen & Ding 2006; Fletcher et al. 2007). On the other hand, if there was sufficient energy in more energetic (say, $\geq 100$ keV) electrons in this flare, the irradiating source would be deeper. We calculated the power of energetic electrons using the hard X-ray data from RHESSI and the thick target model (Brown 1971). (The RHESSI data was not available until 02:29 UT because the satellite was in the night, so we used the data after 02:29 UT.) The electron spectral index was $\sim 4.3$, and the power carried by $\geq 20$ keV electrons was $\sim 3 \times 10^{29}$ erg s$^{-1}$; that carried by $\geq 100$ keV electrons was $\sim 6 \times 10^{27}$ erg s$^{-1}$. In order to compare the energetics, we had to calculate the power radiated in the WL emissions. This required spectral information, which was unknown in the present observation. We leave it for a future study, and only mention that the computed power of electrons is comparable to the X5.3 WLF studied by Metcalf et al. (2003), whose results indicated that high-energy ($\gtrsim 100$ keV) electrons were not sufficient to power the WLF.

### 3.2. *Magnetic Transient*

Transient signals in magnetograms during strong flares have been known for decades (Patterson & Zirin 1981; Zirin & Tanaka 1981; Kosovichev & Zharkova 2001). Some of such signals are indeed irreversible, and hence are probably real magnetic field change (Wang et al. 2002; Yurchyshyn et al. 2004), but those that appear only during the impulsive phase are likely to be an artifact due to distortions of the spectral lines (Patterson 1984; Qiu & Gary 2003). The nature of the latter is still poorly understood because of a lack of spectroscopic observations.

The sign reversal of 6302 $V$ count found in our event was co-spatial and co-temporal with the flare ribbon in 6302 $I$, and hence falls into the latter category. Unfortunately there was no SP observation during the flare, but the full Stokes profiles of this active region were obtained on the previous day. Figure 7 shows the Stokes $I$ and $V$ profiles near the location of the flare ribbon in the northern sunspot, but at 2006 December 12 21:02 UT. The vertical lines indicate the line center and $-120$ mÅ offset; the 6302 $I$ and 6302 $V$ images from FG were taken at $-120$ mÅ. Because of the low temperature in the umbra, the spectral line was already

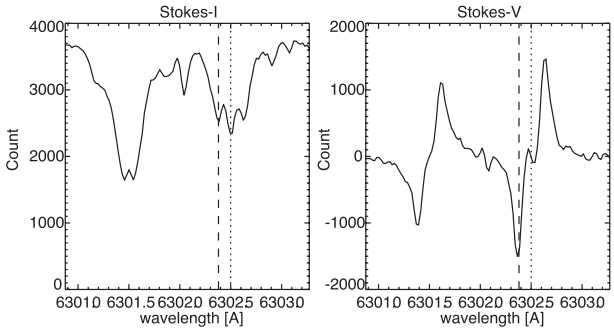


**Fig. 7.** Stokes $I$ and $V$ profiles of the northern sunspot at 2006 December 12 21:02 UT obtained by SOT/SP. The vertical lines indicate the line center (dotted) and $-120$ mÅ offset (dashed).

highly distorted by molecular lines, which made it difficult to determine the continuum level. A conservative estimate of the continuum level is the maximum count in the profile, which is about 3700 in this profile.

In the leading edge where 6302 $V$ showed sign reversal, the 6302 $I$ count increased by about 50%, from $\sim 2500$ to $\sim 3700$. Assuming the same line profile as shown in figure 7, the enhanced count at $-120$ mÅ is comparable to the pre-flare continuum level. We cannot conclude that the line turned to emission, because we do not know the continuum level during the flare, but it is probably fair to say that the line profile was significantly distorted by the flare emission, which caused the "magnetic transient" in this event.

## 4. Conclusions

The high-resolution and seeing-free images from the SOT have revealed the very fine structures in a WLF (more precisely, G band and Fe I 6302 flare). The flare ribbons in the G band and 6302 $I$ clearly show two distinct features: bright and sharp leading edges (kernels) and a following (surrounding) diffuse part. In the diffuse part, the pre-flare structure, such as umbral dots, penumbral filaments, and granules remained visible, giving an impression that the diffuse part was optically thin. The maximum contrast in the flare ribbons was about 600% for the G band and about 50% for 6302 $I$.

Assuming that the leading edge (kernels) was heated directly by nonthermal particles beams, and the diffuse parts were heated heating by radiative back-warming, we made a simple model to derive the depth of the layer of diffuse emission using the intensity profile of the flare ribbon. We found that the layer of diffuse emission is about 100 km below the height of the irradiation source. If the height of initial energy deposition, and hence that of the irradiation source is in the upper chromosphere, as suggested by previous studies (Metcalf et al. 2003; Chen & Ding 2006; Fletcher et al. 2007), our result indicates that the height of the diffuse component, which we believe to be due to radiative back-warming, is also in the upper or middle chromosphere.

The 6302 $V$ images (longitudinal magnetogram) show transient sign reversal, which is probably the same phenomenon known as magnetic transient. The sign reversal was co-spatial and co-temporal with the flare ribbon, and probably due to a significant distortion of the Fe I 6302 line during the flare, though we cannot be conclusive because of a lack of spectroscopic data.

Hinode is a Japanese mission developed and launched by ISAS/JAXA, collaborating with NAOJ as a domestic partner, NASA and STFC (UK) as international partners. Scientific operation of the Hinode mission is conducted by the Hinode science team organized at ISAS/JAXA. This team mainly consists of scientists from institutes in the partner countries. Support for the post-launch operation is provided by JAXA and NAOJ (Japan), STFC (UK), NASA, ESA, and NSC (Norway). This work was carried out at the NAOJ Hinode Science Center, which is supported by the Grant-in-Aid for Creative Scientific Research "The Basic Study of Space Weather Prediction" from MEXT, Japan (Head Investigator: K. Shibata), generous donations from Sun Microsystems, and NAOJ internal funding. HI is supported by a Research Fellowship from the Japan Society of the Promotion of Science for Young Scientists. He also appreciates fruitful comments from H. Hudson, S. Krucker, T. Yokoyama, and an anonymous referee.

## References

Brown, J. C. 1971, Sol. Phys., 18, 489
Chen, Q. R., & Ding, M. D. 2006, ApJ, 641, 1217
Culhane, J. L., et al. 2007, Sol. Phys., 243, 19
Fletcher, L., Hannah, I. G., Hudson, H. S., & Metcalf, T. R. 2007, ApJ, 656, 1187
Golub, L., et al. 2007, Sol. Phys., 243, 63
Hiei, E. 1982, Sol. Phys., 80, 113
Hudson, H. S. 1972, Sol. Phys., 24, 414
Hudson, H. S., Acton, L. W., Hirayama, T., & Uchida, Y. 1992, PASJ, 44, L77
Hudson, H. S., Wolfson, C. J., & Metcalf, T. R. 2006, Sol. Phys., 234, 79
Ichimoto, K., et al. 2007, Sol. Phys. submitted
Kosovichev, A. G., & Zharkova, V. V. 2001, ApJ, 550, L105
Kosugi, T., et al. 2007, Sol. Phys., 243, 3
Kubo, M., et al. 2007, PASJ, 59, S779
Machado, M. E., Emslie, A. G., & Avrett, E. H. 1989, Sol. Phys., 124, 303
Matthews, S. A., van Driel-Gesztelyi, L., Hudson, H. S., & Nitta, N. V. 2003, A&A, 409, 1107
Metcalf, T. R., Canfield, R. C., & Saba, J. L. R. 1990, ApJ, 365, 391
Metcalf, T. R., Alexander, D., Hudson, H. S., & Longcope, D. W. 2003, ApJ, 595, 483
Neidig, D. F. 1989, Sol. Phys., 121, 261
Neidig, D. F., & Kane, S. R. 1993, Sol. Phys., 143, 201
Neidig, D. F., Kiplinger, A. L., Cohl, H. S., & Wiborg, P. H. 1993, ApJ, 406, 306
Patterson, A. 1984, ApJ, 280, 884
Patterson, A., & Zirin, H. 1981, ApJ, 243, L99
Qiu, J., & Gary, D. E. 2003, ApJ, 599, 615
Rust, D. M., & Hegwer, F. 1975, Sol. Phys., 40, 141
Shimizu, T., et al. 2007, Sol. Phys. in press
Suematsu, Y., et al. 2007, Sol. Phys. submitted
Tsuneta, S., et al. 2007, Sol. Phys. submitted
Wang, H., Spirock, T. J., Qiu, J., Haisheng, J., Yurchyshyn, V., Moon, Y.-J., Denker, C., & Goode, P. R. 2002, ApJ, 576, 497
Xu, Y., Cao, W., Lin, C., Yang, G., Jing, J., Denker, C., Emslie, A. G., & Wang, H. 2006, ApJ, 641, 1210
Yurchyshyn, V., Wang, H., Abramenko, V., Spirock, T. J., & Krucker, S. 2004, ApJ, 605, 546
Zirin, H., & Tanaka, K. 1981, ApJ, 250, 791